THE JOURNAL OF PHYSICAL CHEMISTRY B

pubs.acs.org/JPCB Article

Binding-Induced Unfolding of 1-Bromopropane in α-Cyclodextrin

Andres S. Urbina, Victoria M. Boulos, Matthias Zeller, Denilson Mendes de Oliveira, and Dor Ben-Amotz*

Cite This: J. Phys. Chem. B 2020, 124, 11015−11021 Read Online

ACCESS | Metrics & More | Article Recommendations | Supporting Information

ABSTRACT: Raman multivariate curve resolution vibrational spectroscopy and X-ray crystallography are used to quantify changes in the *gauche*−*trans* conformational equilibrium of 1-bromopropane (1-BP) upon binding to α-cyclodextrin (α-CD). Both conformers of 1-BP are found to bind to α-CD, although binding favors the unfolded *trans* conformation. Temperature-dependent measurements of the binding-induced change in the 1-BP conformation equilibrium constant indicate that the *trans* conformer is both enthalpically and entropically stabilized in the host cavity.

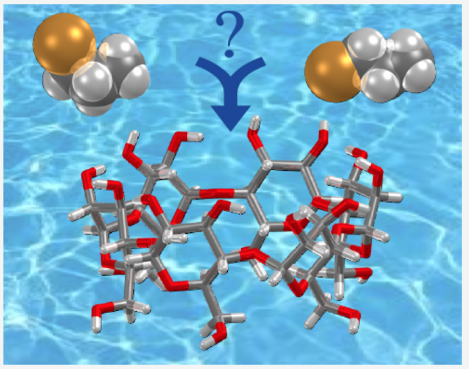

INTRODUCTION

Binding-induced conformational changes play an important role in a wide range of biochemical and pharmaceutical processes,[1−7] although the conventional lock-and-key picture of host−guest binding implicitly neglects the influence of conformational flexibility on binding affinity. Some previous experimental and theoretical studies have reported evidence of guest conformational changes upon binding to a host cavity[6−10] but have not quantified the associated binding-induced conformational equilibrium constant and thermodynamic changes or compared the corresponding complex structures in the solid and aqueous solution states. Here, we do so by performing Raman multivariate curve resolution (Raman-MCR) and X-ray crystallographic measurements of the binding of 1-bromopropane (1-BP) to α-cyclodextrin (α-CD). Our results reveal that the guest *gauche*−*trans* conformational equilibrium shifts toward the *trans* conformer upon binding (although both conformers are present in the bound complex) and is essentially the same in the solid and aqueous systems. Moreover, temperature-dependent Raman measurements of the solid complex reveal that the binding-induced unfolding of 1-BP is both enthalpically and entropically favored. Thus, the present results provide a quantitative illustration of the importance of relaxing the simple lock-and-key picture of host−guest binding to include conformational flexibility and the associated entropic contributions to binding affinities.

Several previous studies of guest conformation changes have involved synthetic nanocapsule hosts. These include NOESY and COSY nuclear magnetic resonance (NMR) experimental and molecular dynamics simulation studies of the folding and helix formation of long alkanes trapped in cavitand nanocapsule complexes and nanotubes.[9−13] Cyclodextrins, which are biologically produced hosts widely used in drug delivery and other supramolecular assembly applications,[14−16] have also been found to induce guest conformational changes,[17] probed using various NMR methods[18,19] and vibrational spectroscopy.[20,21]

Raman-MCR provides a means of decomposing the Raman spectrum of a solution into solvent and solute-correlated (SC) spectral components. The latter SC component contains intramolecular solute vibrational bands, as well as more subtle information arising from solute−solvent interactions and conformational flexibility, including changes in *gauche*−*trans* equilibrium constants.[22] The present Raman-MCR measurements are facilitated by the fact that the *gauche* and *trans* conformers have well-resolved C−Br stretch peaks near 560 and 640 cm^{-1}, respectively.[23] Unlike prior studies that have used Raman-MCR to measure solute hydration-shell O−H band spectra,[24] here we use binding-induced changes in the guest C−Br and C−H stretch band intensities to both confirm host−guest binding and quantify binding-induced changes in the 1-BP *gauche*−*trans* equilibrium. More specifically, SC spectra of the free and bound aqueous host and guest molecules have been obtained using self-modeling curve

Received: September 22, 2020
Revised: November 2, 2020
Published: November 18, 2020

https://dx.doi.org/10.1021/acs.jpcb.0c08630
J. Phys. Chem. B 2020, 124, 11015−11021

resolution (SMCR)[22,24−27] (see the Methods section for further details).

METHODS

Preparation of Aqueous Solutions. Saturated aqueous solutions of 1-BP (99.5+%, Sigma-Aldrich) were prepared by gently adding 2 mL of water (18.2 MΩ cm resistivity, Milli-Q UF Plus) or a 20 mM aqueous solution of α-CD (99.5+%, TCI) into a glass cuvette that already contained 50 μL of 1-BP. Thus, all saturated 1-BP solutions contained two liquid phases consisting of a 1-BP-rich droplet (at the bottom of the cell) surrounded by the aqueous phase and stored for at least 48 h in order to allow 1-BP to saturate the aqueous phase to its solubility limit of approximately 20 mM free 1-BP.[28] When the aqueous solution contained α-CD, after sitting for 3 days or more, crystals of different sizes were observed to grow at the meniscus between the aqueous and 1-BP phases. It is such crystals that were analyzed using X-ray diffraction and found to contain a solid one-to-one complex of 1-BP in α-CD.

Raman Spectroscopy. Unless stated otherwise, two replicate 5 min spectra were obtained using a 514.5 nm Ar-ion excitation laser with ∼20 mW at the sample, as previously described.[26] Liquid and gas samples (in a 12 mm round glass vial) and pure α-CD powder (in a melting-point capillary) were tightly fit within a 1 cm copper block held at 20 °C, and crystals of the α-CD-1-BP complex were mounted on the copper block. Pure liquid and solid spectra were obtained using two 1 min replicates.

Raman-MCR. SMCR[25] was used to decompose solution and solvent spectra into solvent and SC components.[22,24,26,27] The SC spectra of saturated 1-BP in an aqueous 20 mM α-CD were obtained using an aqueous 20 mM α-CD solution as the solvent reference spectrum.

Single-Crystal X-ray Diffraction. A suitable single crystal (∼0.4 mm cubed) of the α-CD-1-BP complex was taken directly from the biphasic crystallization setup, quickly coated with a trace of Fomblin oil, and transferred directly into the cold stream of a goniometer head of a Bruker QUEST diffractometer with a fixed chi angle, a Mo Kα wavelength (λ = 0.71073 Å) sealed fine focus X-ray tube, a single-crystal curved graphite incident beam monochromator, and a PHOTON 100 CMOS area detector equipped with an Oxford Cryosystems low-temperature device. Examination and data collection were performed at 150 K (see the Supporting Information for further details).

Density Functional Theory Calculations. Density functional theory (DFT) calculations of different 1-BP systems were performed using the Gaussian 16 suite of programs.[29] Geometry optimizations along with Raman spectra were calculated. For the bound 1-BP species, geometries of 1:1 complexes were taken from the most probable configurations, as obtained from the X-ray diffraction measurements for each conformer. Two levels of theory were used, B3LYP/6-31g(d,p) and WB97/LANL2DZ. The systems studied and the corresponding results are shown in Tables S1 and S2 in the Supporting Information.

Isomerization Equilibrium. The analysis of the isomerization equilibrium was performed in the C−Br stretch-band region. The areas of the bands were determined after background subtraction either by integrating the bands to the left and right side of the minimum between the two bands or from the ratio of the areas of Gaussian or Voigt functions independently fit the two bands, avoiding the region in which they overlap. For both free and mixed (bound + free) 1-BP, seven spectra from independent experiments were obtained and the bands were analyzed using the above area estimation methods. The reported area ratios for free and bound 1-BP correspond to the average and standard deviation of a set of 21 area ratios that were obtained for each system at 20 °C. For pure liquid 1-BP, four independent spectra were collected and analyzed in the same way. The spectrum of the bound 1-BP species in the solid crystal was obtained from the difference between the spectra of α-CD-1-BP crystal and α-CD powder (see the Supporting Information and Figure S1 for more information). Unpolarized Raman spectra were collected from four different orientations/regions of the solid samples, with no attempt to orient the crystals, and the corresponding bound 1-BP spectra were used to obtain the corresponding *gauche*−*trans* area ratios of 1-BP bound in α-CD.

RESULTS AND DISCUSSION

Figure 1a shows the measured Raman spectra of water, a 20 mM solution of α-CD, and saturated solutions of 1-BP in water

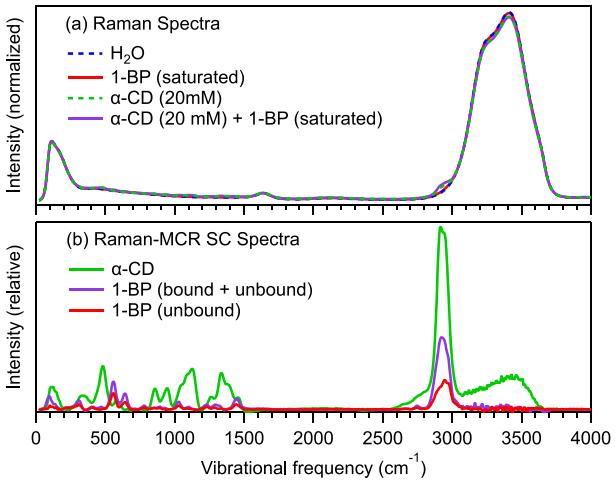

Figure 1. Raman spectra in (a), all normalized to the same area, are used to obtain the Raman-MCR SC spectra in (b) for unbound aqueous α-CD (green) and 1-BP (red), as well as an equilibrium mixture (purple) of free and bound 1-BP in a 20 mM α-CD solution saturated with 1-BP.

and in 20 mM aqueous α-CD at 20 °C. Note that 1-BP was maintained at its saturation concentration by immersing a droplet of liquid 1-BP in the corresponding aqueous solutions. All Raman spectra shown in Figure 1a look very similar to those of pure water except for a small shoulder on the left side of the O−H stretching band due primarily to the C−H stretch of α-CD. The resulting Raman-MCR SC spectra shown in Figure 1b are more revealing, as they uncover multiple intramolecular vibrational bands of both α-CD and 1-BP. Specifically, the red curve represents the SC spectrum of unbound 1-BP, the purple curve corresponds to the SC spectrum of a mixture of bound and unbound 1-BP, and the green curve is the SC spectrum of α-CD in water. The latter α-CD spectral features are not present in the bound 1-BP spectrum, as they were effectively subtracted away by the SMCR spectral decomposition process in which the solution contains both 1-BP and α-CD and the solvent contains only α-CD, both with the same α-CD concentration of ∼20 mM. The increase, by nearly a factor of 2, of the 1-BP band intensities in

https://dx.doi.org/10.1021/acs.jpcb.0c08630
J. Phys. Chem. B 2020, 124, 11015−11021

the presence of α-CD (compare the purple and red spectra) clearly reveals that the α-CD binding induced an increase in the solubility of 1-BP. Note that this factor of 2 is a lower bound to the actual binding-induced solubilization of 1-BP, as both our experimental and theoretical results indicated that the Raman cross section of bound 1-BP is smaller than that of 1-BP dissolved in water (see the Supporting Information for further details).

Figure 2 shows an expanded view of the C−Br stretch bands for the two conformers of 1-BP in a saturated aqueous solution

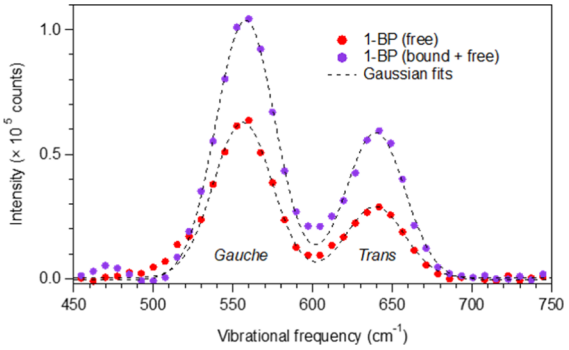

Figure 2. Raman-MCR SC spectra in the C−Br stretch region. The points are the experimental intensities and the dashed curves are the sum of Gaussian fits to the two sub-bands.

(red) and in a solution containing 20 mM α-CD (purple), along with the associated fits to a superposition of two Gaussians. The assignment of these peaks to the *gauche* (at ∼560 cm^{-1}) and *trans* (at ∼650 cm^{-1}) isomers are confirmed both by the disappearance of the *gauche* peak upon freezing pure 1-BP,[30] as well as our own (and prior)[31] quantum calculations (see the Methods section and Supporting Information). The associated *gauche* and *trans* band areas, A_G and A_T, may be obtained either by directly integrating the experimental spectra to the left and right of the minimum between the two bands or from the areas of the corresponding Gaussian (or Voigt) fits to the experimental bands, and the resulting band area ratios agree to within ∼5%. All of the reported equilibrium constant (K_{eq}) values are average values obtained using three different area measurement methods (see the Methods section for further details). The band area of each conformer may be expressed as $A_i = c_i\sigma_i$, where c_i and σ_i are the concentration and Raman scattering cross section of the ith conformer, respectively. Therefore, the equilibrium constant is $K_{eq} = c_G/c_T = (A_G/\sigma_G)/(A_T/\sigma_T)$. Importantly, quantum calculations indicate that the two conformers have approximately the same C−Br Raman cross section ratio, $\sigma_G/\sigma_T \sim 1$, both in the gas phase and in a dielectric implicit aqueous solvent, and thus the ratio of the band areas provides a spectroscopic measure of K_{eq} (see the Methods section and Supporting Information for additional details). However, our quantum calculations also indicate that the C−Br Raman cross sections decrease upon binding and have a significantly different ratio of $\sigma_G/\sigma_T \sim 3$, thus also influencing the measured isomerization free energy and entropy, as further discussed below. It is also noteworthy that the influence of host−guest binding on molecular polarizabilities and optical spectra have previously been described[32] but not, to our knowledge, with regard to Raman cross sections or the associated changes in polarizability with respect to the corresponding vibrational and conformational degrees of freedom.

If we assume that binding does not change the Raman scattering cross section ratio, $\sigma_G/\sigma_T \sim 1$, then the isomerization equilibrium constant for the 1-BP bound to α-CD, obtained from the difference between the purple and red band areas in Figure 2, implies that $K_{eq} \sim 1.4 \pm 0.3$, which is nearly a factor of 2 smaller than that of 1-BP dissolved in water, $K_{eq} \sim 2.3 \pm 0.2$. However, our DFT calculations of the 1-BP isomers bound in α-CD indicate that the Raman scattering cross section of the bound *gauche* conformer is three times larger than the bound *trans* conformer and thus $\sigma_G/\sigma_T \sim 3$ (see the Methods section and Supporting Information for additional details). If we use this predicted cross section ratio, then the inferred conformational equilibrium constant further decreases to $K_{eq} \sim 0.5 \pm 0.2$ in the bound host−guest complex. In either case, the decrease in K_{eq} upon transfer from the aqueous solution to the α-CD cavity implies that the 1-BP conformation equilibrium shifts toward the *trans* conformer upon binding to α-CD. Moreover, our additional Raman measurements of the solid complex imply that the conformation equilibrium constant is approximately the same in the solid state as it is for the complex dissolved in liquid water (as further described below).

Figure 3 compares C−Br stretch bands of 1-BP in the pure liquid (a), aqueous solution (b), and bound in α-CD in the

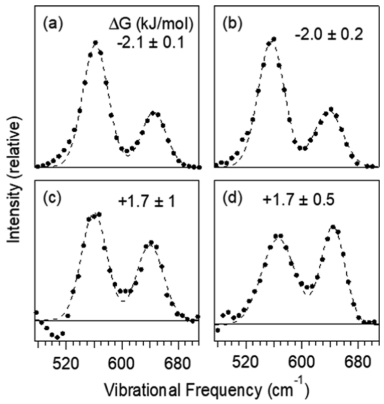

Figure 3. Raman spectra (and Gaussian fits) of the 1-BP C−Br stretch bands obtained for different systems and the corresponding free energy $\Delta G = -RT \ln K_{eq}$ at 293.15 K. (a) Pure liquid 1-BP ($K_{eq} \sim 2.4 \pm 0.1$), (b) aqueous 1-BP ($K_{eq} \sim 2.3 \pm 0.2$), (c) 1-BP bound to α-CD in the aqueous solution ($K_{eq} \sim 0.5 \pm 0.2$) and (d) in the solid crystal ($K_{eq} \sim 0.5 \pm 0.1$). Note that the above ΔG values in (c,d) were obtained assuming $\sigma_G/\sigma_T \sim 3$ (as discussed in the text).

aqueous (c) and solid (d) complexes, along with the corresponding partial molar Gibbs free-energy change $\Delta G = -RT \ln K_{eq}$ for the *trans* to *gauche* isomerization process. The ΔG values shown in panels (a,b) are within ±0.2 kJ/mol of previously reported Raman-based experimental results in pure liquid[33,34] and aqueous[35] 1-BP. The bound 1-BP spectra in panels (c,d) were obtained from the difference between the bound and unbound spectra assuming $\sigma_G/\sigma_T \sim 3$ (as explained above, with further details provided in the Methods section and Supporting Information). Note that the negative-going feature in panel (c) is a subtraction artifact resulting from the large α-CD peak near 480 cm^{-1} (see Figure 1). Fine-tuning the subtraction to minimize this artifact does not significantly alter the resulting K_{eq} (and ΔG).

https://dx.doi.org/10.1021/acs.jpcb.0c08630
J. Phys. Chem. B 2020, 124, 11015−11021

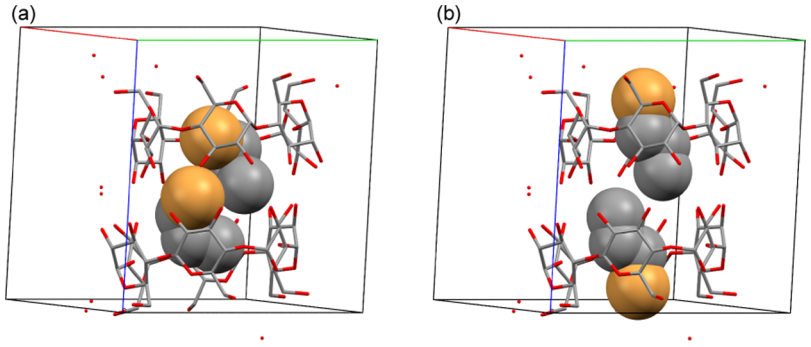

Figure 4. (a) View of the α-CD-1-BP dimer showing the most probable *gauche* configurations [10.4(2) and 17.5(2) %]. (b) View of the α-CD-1-BP dimer showing the most probable *trans* configurations [28.8(4) and 51.5(4) %]. The red, green, and blue lines point along the a, b and c axes, respectively (see the SI for further details).

To gain further insight into the distribution of *gauche* and *trans* isomers inside the α-CD molecules, we also analyzed crystalline samples of the host−guest complex using single-crystal X-ray diffraction. The overall packing and arrangement of the constituent entities in the crystal structure are dominated by the α-CD molecules connected to each other through a hydrogen-bonding network between the hydroxyl moieties of neighboring molecules creating a dense packing that leaves no open space other than the interior of the cylindrical α-CD molecules. The observed structures differ from that of native α-CD but are closely related to a series of other guest hosting α-CD complexes. A search of the Cambridge structural database[36] revealed several α-CD host−guest complexes with acetone,[37] thiophene,[38] diethylfumarate,[39] hemikis(2,2′-azodipyridine),[40] *n*-butylisothiocyanate,[41] lithium triiodide iodine,[42] and various metallocene complexes having unit cell shapes and α-CD packing that differ from the α-CD-1-BP complex only by the nature of the guests in the cavity. Both α-CD-1-BP and its isomorphous counterparts are characterized by a stacking arrangement of α-CD molecules with the unit cell having two α-CD molecules forming a head to head dimer (capsule). Molecules line up in such a way that the interior voids of the cylindrical α-CD molecules connect to form channels extending through the crystal along the c-axis of the unit cell (Figure 4.).

Single-crystal X-ray diffraction provides an average of the arrangement of all constituent entities over the entire crystal (in the form of the electron densities inside the crystallographic repeat units, the unit cell). If positions of atoms or fragments differ between unit cells, then disorder has to be included when building the structural model based on the diffraction data. Two different types of disorder are observed in the structure: (1) the two-fold disorder of a water molecule, inducing disorder of two of twelve crystallographically independent α-CD sugar moieties (see the Supporting Information for details regarding this disorder) and (2) the disorder associated with the two conformations of 1-BP embedded in the cavities of the two α-CD molecules in each unit cell, as described in greater detail below (and in the Supporting Information).

Figure 4 shows representative unit cell structures obtained from the α-CD-1-BP single-crystal X-ray diffraction analysis. Figure 4a shows the most probable bound *gauche* conformers, while Figure 4b shows the most probable bound *trans* conformers. Note that although (a) has two *gauche* and (b) has two *trans* 1-BP molecules, the X-ray results do not imply that the structures are invariably paired in this way. In other words, the X-ray structures are equally consistent with unit cell structures in which neighboring α-CD hosts contain different 1-BP conformers.

More specifically, the single-crystal data indicate that in the crystal, each α-CD molecule contains exactly one bound 1-BP molecule disordered over several slightly shifted and rotated positions of both the *trans* and *gauche* conformations. Major moiety disordered molecules as well as their assignment as *gauche* or *trans* were immediately evident from difference electron density maps and were assigned and modeled. This was followed by re-analysis of difference density maps and assignment of successively less prevalent disordered moieties until the remaining difference electron density maps were essentially featureless. In total, six conformations were modeled for each of the 1-BP molecule in the two-independent α-CD molecules with refined occupancies between 0.515(4) and 0.0561(19). All 1-BP molecules are clearly associated with one of the two α-CD molecules, with no 1-BP molecules stretching along the channel between the two α-CD hosts. Total occupancies for all disordered moieties refined to close to unity for each site, indicating the absence of empty or water-filled α-CD cavities. In the final refinement cycle, the total occupancy was constrained to exactly one. In the crystal structure, measured at 150 K, the *trans* conformation is significantly favored (as further discussed below).

After applying structural restraints to the 1-BP molecules embedded inside the α-CD dimer (see the Supporting Information for details), the 1-BP molecules in the two α-CD structures had *gauche*−*trans* ratios of 0.26/0.74 and 0.35/0.65 at 150 K, giving an average $K_{eq} \sim 0.3/0.7 \sim 0.4 \pm 0.1$ (with error bars obtained from the ±0.05 difference between the individual conformer probabilities in the first and second crystallographically distinct structures). This slightly smaller value of K_{eq} at 150 K, relative to the $K_{eq} \sim 0.5$ for the bound complex at 293 K, is consistent with positive ΔH for the *trans* to *gauche* conformation change in the α-CD host. The positive sign of ΔH is also consistent with the following temperature-dependent Raman measurements of the conformer peak ratio in the solid complex.

Figure 5 shows results obtained from temperature-dependent measurements of the 1-BP *trans* to *gauche* (folding) equilibrium constant to obtain the corresponding isomerization ΔH and ΔS values. Specifically, the *trans* to *gauche* enthalpy and entropy changes are obtained from the corresponding temperature-dependent ΔG values using $\Delta H = [\partial(\Delta G/T)/\partial(1/T)]_P$ and $\Delta S = (\partial \Delta G/\partial T)_P$. The error associated with such temperature-dependent measurements

https://dx.doi.org/10.1021/acs.jpcb.0c08630
J. Phys. Chem. B 2020, 124, 11015−11021

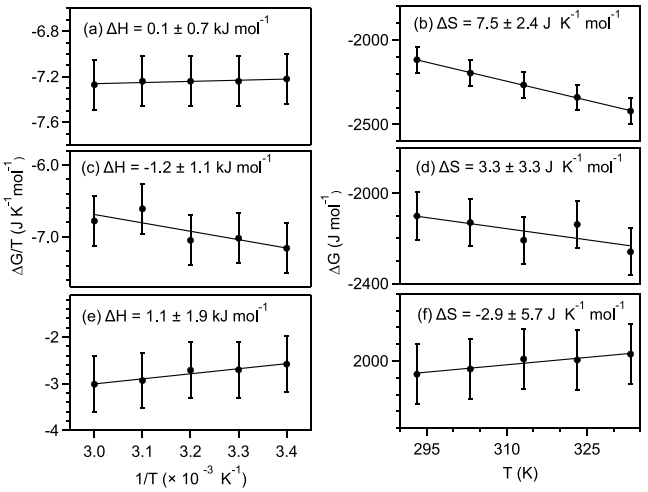

Figure 5. Experimental isomerization (*trans* to *gauche*) enthalpy and entropy for 1-BP for pure liquid 1-BP (a,b), aqueous 1-BP (c,d), and α-CD-1-BP complex in the crystalline solid state (e,f). Note that the $-T\Delta S$ entropic contributions to ΔG at 293.15 K range from -2.2 ± 0.7 kJ/mol in the pure 1-BP liquid to -1.0 ± 1.0 kJ/mol in the aqueous solution. In the case of bound 1-BP, at 293.15 K, the entropic contribution is -1.8 ± 1.7 kJ mol^{-1}, assuming $\sigma_G/\sigma_T \sim 1$ or 0.9 ± 1.8 kJ mol^{-1}, assuming $\sigma_G/\sigma_T \sim 3$.

correspond to uncertainties of $\pm 1-2$ kJ/mol in ΔH and $\pm 2-6$ J K^{-1} mol^{-1} in ΔS (with an additional uncertainty in ΔS resulting from the Raman cross section ratio, as further discussed below).

In spite of the significant uncertainties associated with the isomerization enthalpy, the ΔH of ~0.1 kJ/mol for 1-BP in the pure liquid is within the range of the previously reported values, varying between 0.1 kJ/mol < ΔH < 1.1 kJ/mol.[43−45] More interestingly, our results indicate that the *trans* to *gauche* ΔH changes sign upon binding to α-CD. Specifically, ΔH is negative for 1-BP dissolved in water but becomes positive upon binding to α-CD, while the sign ΔS changes from positive to negative upon binding. This implies that the *trans* conformer has both an enthalpically and entropically more favorable interaction with the α-CD cavity.

The conformational ΔS change is more difficult to accurately quantify than ΔH both because of its small magnitude (relative to the error bars of the associated data points) and because, unlike ΔH, the value of the experimentally inferred ΔS is sensitive to binding-induced changes in the relative Raman cross section of the two conformers. Note that the unbound ΔS values in Figure 5b,d are positive and, within experimental error, have the same magnitude as $\Delta S = R \ln 2 \approx 6$ J K^{-1} mol^{-1} obtained assuming that the entropy changes are entirely due to the fact that there are two *gauche* conformers and only one *trans* conformer.[23,46] Deviations from this value may arise from various sources, including differences between the internal partition functions of the two isomers, as well as the surrounding host and/or solvent molecules. However, the bound ΔS value in Figure 5f, obtained assuming that $\sigma_G/\sigma_T \sim 3$, has the opposite sign, implying that the bound *trans* conformer has more thermally accessible configurations than the *gauche* conformation. Thus, the binding-induced sign change of ΔS is consistent with a looser fit of the *trans* conformer to the α-CD cavity, while the sign change of ΔH implies that the tighter fit of the *gauche* conformer to α-CD cavity has a greater repulsive interaction with the cavity walls.

It is also noteworthy that $\Delta G \sim 1.1 \pm 0.3$ kJ mol^{-1} for the folding of 1-BP in α-CD at 150 K, obtained directly from the X-ray crystal diffraction analysis, is roughly consistent with the value of $\Delta G \sim 1.5 \pm 6.0$ kJ mol^{-1} obtained from $\Delta S \sim -2.9$ J K^{-1} mol^{-1} (assuming $\sigma_G/\sigma_T \sim 3$) and $\Delta H \sim 1.1$ kJ/mol, when extrapolated down to 150 K. The approximate agreement between the latter two ΔG values for bound 1-BP at 150 K implies that ΔS and ΔH remain approximately temperature independent between 150 and 335 K and provides additional support for the prediction that $\sigma_G/\sigma_T \sim 3$ for 1-BP bound within the α-CD cavity.

CONCLUSIONS

In summary, Raman-MCR and X-ray crystallographic measurements reveal that 1-BP remains flexible upon binding to α-CD, although its conformation equilibrium is shifted toward the unfolded *trans* conformation upon binding. Our experimental temperature-dependent Raman measurements on both free and α-CD-bound 1-BP, combined with our predicted binding-induced Raman cross section changes, imply that both the conformational enthalpy and entropy of 1-BP change sign upon binding to α-CD. The latter sign changes, as well as the corresponding conformational free energy, are all consistent with a more favorable fit of the *trans* conformer to the α-CD cavity.

ASSOCIATED CONTENT

Supporting Information

The Supporting Information is available free of charge at https://pubs.acs.org/doi/10.1021/acs.jpcb.0c08630.

Raman spectra of the solid α-CD-1-BP crystal; generation of difference spectrum corresponding to bound 1-BP species present in the crystal; predicted *gauche-trans* Raman cross-section ratios; frequencies and Raman activities calculated at two levels of theory for different 1-BP systems; gauche-trans Raman cross-section ratio predicted at two levels of theory; binding-induced C-Br Raman cross-section changes; Raman cross-section change of the C-Br stretching mode of both the gauche and trans conformers upon binding to α-CD; gas phase 1-BP Raman spectra and thermodynamics; ; Raman spectra of gaseous 1-BP in the C-Br stretch region at different temperatures; vapor pressure vs. area of the C-Br bands; experimental isomerization (*trans* to *gauche*) entropy and enthalpy for gaseous 1-BP; and details of the single-crystal X-Ray diffraction experiment. Supplementary crystallographic data for this paper is available free of charge from the Cambridge Crystallographic Data Centre *via* www.ccdc.cam.ac.uk/data_request/cif (CCDC 2023037) (PDF)

AUTHOR INFORMATION

Corresponding Author

Dor Ben-Amotz − *Department of Chemistry, Purdue University, West Lafayette, Indiana 47907, United States;* orcid.org/0000-0003-4683-5401; Email: bendor@purdue.edu

Authors

Andres S. Urbina − *Department of Chemistry, Purdue University, West Lafayette, Indiana 47907, United States;* orcid.org/0000-0001-6482-4736

Victoria M. Boulos − *Department of Chemistry, Purdue University, West Lafayette, Indiana 47907, United States*

Matthias Zeller − *Department of Chemistry, Purdue University, West Lafayette, Indiana 47907, United States;* orcid.org/0000-0002-3305-852X

Denilson Mendes de Oliveira − *Department of Chemistry, Purdue University, West Lafayette, Indiana 47907, United States;* orcid.org/0000-0002-2579-8405

Complete contact information is available at: https://pubs.acs.org/10.1021/acs.jpcb.0c08630

Notes

The authors declare no competing financial interest.

■ ACKNOWLEDGMENTS

This material is based upon work supported by the National Science Foundation under grant no. CHE-1763581 to D.B.A., A.S.U., and D.M.O., and through the Major Research Instrumentation Program under grant no. CHE-1625543 (Funding for the single-crystal X-ray diffractometer).

■ REFERENCES

(1) Koshland, D. E. Conformational changes: How small is big enough? *Nat. Med.* **1998**, *4*, 1112−1114.

(2) Mesecar, A. D.; Stoddard, B. L.; Koshland, D. E. Orbital steering in the catalytic power of enzymes: Small structural changes with large catalytic consequences. *Science* **1997**, *277*, 202.

(3) Ahmad, E.; Rabbani, G.; Zaidi, N.; Khan, M. A.; Qadeer, A.; Ishtikhar, M.; Singh, S.; Khan, R. H. Revisiting ligand-induced conformational changes in proteins: Essence, advancements, implications and future challenges. *J. Biomol. Struct. Dyn.* **2013**, *31*, 630−648.

(4) Ahmad, M.; Helms, V.; Kalinina, O. V.; Lengauer, T. The role of conformational changes in molecular recognition. *J. Phys. Chem. B* **2016**, *120*, 2138−2144.

(5) Chiarparin, E.; Packer, M. J.; Wilson, D. M. Experimental free ligand conformations: A missing link in structure-based drug discovery. *Future Med. Chem.* **2019**, *11*, 79−82.

(6) van Zundert, G. C. P.; Hudson, B. M.; de Oliveira, S. H. P.; Keedy, D. A.; Fonseca, R.; Heliou, A.; Suresh, P.; Borrelli, K.; Day, T.; et al. Qfit-ligand reveals widespread conformational heterogeneity of drug-like molecules in x-ray electron density maps. *J. Med. Chem.* **2018**, *61*, 11183−11198.

(7) Mobley, D. L.; Dill, K. A. Binding of small-molecule ligands to proteins: "What you see" is not always "what you get". *Structure* **2009**, *17*, 489−498.

(8) Sasmal, S.; Gill, S. C.; Lim, N. M.; Mobley, D. L. Sampling conformational changes of bound ligands using nonequilibrium candidate monte carlo and molecular dynamics. *J. Chem. Theory Comput.* **2020**, *16*, 1854−1865.

(9) Gibb, C. L. D.; Gibb, B. C. Straight-chain alkanes template the assembly of water-soluble nano-capsules. *Chem. Commun.* **2007**, 1635−1637.

(10) Scarso, A.; Trembleau, L.; Rebek, J. Helical folding of alkanes in a self-assembled, cylindrical capsule. *J. Am. Chem. Soc.* **2004**, *126*, 13512−13518.

(11) Velpuri, S. V. V.; Gade, H. M.; Wanjari, P. P. Encapsulation driven conformational changes in n-alkanes inside a hydrogen-bonded supramolecular cavitand assembly. *Chem. Phys.* **2019**, *521*, 100−107.

(12) Wanjari, P. P.; Sangwai, A. V.; Ashbaugh, H. S. Confinement induced conformational changes in n-alkanes sequestered within a narrow carbon nanotube. *Phys. Chem. Chem. Phys.* **2012**, *14*, 2702−2709.

(13) Rebek, J. Molecular behavior in small spaces. *Acc. Chem. Res.* **2009**, *42*, 1660−1668.

(14) Davis, M. E.; Brewster, M. E. Cyclodextrin-based pharmaceutics: Past, present and future. *Nat. Rev. Drug Discovery* **2004**, *3*, 1023−1035.

(15) Kolesnichenko, I. V.; Anslyn, E. V. Practical applications of supramolecular chemistry. *Chem. Soc. Rev.* **2017**, *46*, 2385−2390.

(16) Geng, W.-C.; Sessler, J. L.; Guo, D.-S. Supramolecular prodrugs based on host−guest interactions. *Chem. Soc. Rev.* **2020**, *49*, 2303−2315.

(17) Connors, K. A. The stability of cyclodextrin complexes in solution. *Chem. Rev.* **1997**, *97*, 1325−1358.

(18) Schneider, H.-J.; Hacket, F.; Rüdiger, V.; Ikeda, H. Nmr studies of cyclodextrins and cyclodextrin complexes. *Chem. Rev.* **1998**, *98*, 1755−1786.

(19) Inoue, Y. Nmr studies of the structure and properties of cyclodextrins and their inclusion complexes. In *Annual reports on nmr spectroscopy*, Webb, G. A., Ed.; Academic Press, 1993; Vol. *27*; pp 59−101.

(20) Amado, A. M.; Ribeiro-Claro, P. J. A. Selection of substituted benzaldehyde conformers by the cyclodextrin inclusion process: A raman spectroscopic study. *J. Raman Spectrosc.* **2000**, *31*, 971−978.

(21) Lamcharfi, E.; Kunesch, G.; Meyer, C.; Robert, B. Investigation of cyclodextrin inclusion compounds using ft-ir and raman spectroscopy. *Spectrochim. Acta, Part A* **1995**, *51*, 1861−1870.

(22) Perera, P.; Wyche, M.; Loethen, Y.; Ben-Amotz, D. Solute-induced perturbations of solvent-shell molecules observed using multivariate raman curve resolution. *J. Am. Chem. Soc.* **2008**, *130*, 4576−4577.

(23) Hu, M.-H. A.; de Souza, L. E. S.; Lee, M.-R.; Ben-Amotz, D. Pressure and temperature-dependent gauche-trans isomerization of 1-bromopropane: Raman measurement and statistical thermodynamic analysis. *J. Chem. Phys.* **1999**, *110*, 2498−2507.

(24) Ben-Amotz, D. Hydration-shell vibrational spectroscopy. *J. Am. Chem. Soc.* **2019**, *141*, 10569−10580.

(25) Lawton, W. H.; Sylvestre, E. A. Self-modeling curve resolution. *Technometrics* **1971**, *13*, 617−633.

(26) Davis, J. G.; Gierszal, K. P.; Wang, P.; Ben-Amotz, D. Water structural transformation at molecular hydrophobic interfaces. *Nature* **2012**, *491*, 582.

(27) Wu, X.; Lu, W.; Streacker, L. M.; Ashbaugh, H. S.; Ben-Amotz, D. Temperature-dependent hydrophobic crossover length scale and water tetrahedral order. *J. Phys. Chem. Lett.* **2018**, *9*, 1012−1017.

(28) Yalkosky, S. H., He, Y.; Jain, P. *Handbook of aqueous solubility data*. 2 ed.; CRC Press: Boca Raton, FL, 2016.

(29) Frisch, M. J.; Trucks, G. W.; Schlegel, H. B.; Scuseria, G. E.; Robb, M. A.; Cheeseman, J. R.; Scalmani, G.; Barone, V.; Petersson, G. A., et al. *Gaussian 16*, Revision C.01; Gaussian, Inc.: Wallingford, CT, 2016.

(30) Ogawa, Y.; Imazeki, S.; Yamaguchi, H.; Matsuura, H.; Harada, I.; Shimanouchi, T. Vibration spectra and rotational isomerism of chain molecules. Vii. 1-chloro-, 1-bromo-, and 1-iodopropanes, and 1-chloro-, 1-bromo-, and 1-iodobutanes. *Bull. Chem. Soc. Jpn.* **1978**, *51*, 748−767.

(31) Durig, J. R.; Zhu, X.; Shen, S. Conformational and structural studies of 1-chloropropane and 1-bromopropane from temperature-dependant ft-ir spectra of rare gas solutions and ab initio calculations. *J. Mol. Struct.* **2001**, *570*, 1−23.

(32) Marquez, C.; Nau, W. M. Polarizabilities inside molecular containers. *Angew. Chem., Int. Ed.* **2001**, *40*, 4387−4390.

(33) Yoshino, T.; Bernstein, H. J. Internal rotation: Ix. The infrared and raman spectra of liquid normal alkyl bromides. *Can. J. Chem.* **1957**, *35*, 339−344.

(34) Katō, M.; Taniguchi, Y. Effect of pressure on conformational equilibria of liquid 1-chloropropane and 1-bromopropane. *J. Chem. Phys.* **1990**, *93*, 4345−4348.

(35) Kasezawa, K.; Kato, M. Effect of pressure on conformational equilibria of 1-chloropropane and 1-bromopropane in water and organic solvents: A raman spectroscopic study. *J. Phys. Chem. B* **2009**, *113*, 8607−8612.
(36) Groom, C. R.; Allen, F. H. The cambridge structural database in retrospect and prospect. *Angew. Chem., Int. Ed.* **2014**, *53*, 662−671.
(37) Nicolis, I.; Villain, F.; Coleman, A. W.; Rango, C. d. X-ray crystallographic structure of the two-to-one α-cyclodextrin-acetone. 9h2o compound. *Supramol. Chem.* **1994**, *3*, 251−259.
(38) Takashima, Y.; Sakamoto, K.; Oizumi, Y.; Yamaguchi, H.; Kamitori, S.; Harada, A. Complex formation of cyclodextrins with various thiophenes and their polymerization in water: Preparation of poly-pseudo-rotaxanes containing poly(thiophene)s. *J. Inclusion Phenom. Macrocyclic Chem.* **2006**, *56*, 45−53.
(39) Choi, S.; Frank, W.; Ritter, H. Novel polymerization of diethyl fumarate and maleate in aqueous media via cyclodextrin-complexes. *React. Funct. Polym.* **2006**, *66*, 149−156.
(40) Gu, Z.-Y.; Guo, D.-S.; Liu, Y. Guest releasing from solution to solid-state triggered by cyclomaltohexaose (alpha-cyclodextrin) aggregation. *Carbohydr. Res.* **2010**, *345*, 2670−2675.
(41) Sicard-Roselli, C.; Perly, B.; Le Bas, G. The respective benefits of x-ray crystallography and nmr for the structural determination of the inclusion complex between butyl-isothiocyanate and alpha-cyclodextrin. *J. Inclusion Phenom. Macrocyclic Chem.* **2001**, *39*, 333−337.
(42) Noltemeyer, M.; Saenger, W. Topography of cyclodextrin inclusion complexes. 12. Structural chemistry of linear alpha-cyclodextrin-polyiodide complexes - x-ray crystal-structures of (alpha-cyclodextrin)1.Lii3.I2.8h2o and (alpha-cyclodextrin)-2.Cd0.5.I5.27h2o - models for the blue amylose-iodide complex. *J. Am. Chem. Soc.* **1980**, *102*, 2710−2722.
(43) Yoshiki, O.; Shuji, I.; Hiroko, Y.; Hiroatsu, M.; Issei, H.; Takehiko, S. Vibration spectra and rotational isomerism of chain molecules. Vii. 1-chloro-, 1-bromo-, and 1-iodopropanes, and 1-chloro-, 1-bromo-, and 1-iodobutanes. *Bull. Chem. Soc. Jpn.* **1978**, *51*, 748−767.
(44) Anderson, M. W.; Taylor, J. A.; Walker, C. T. Energy difference of the trans−gauche c−br configurations in several 1-bromoalkanes. *J. Chem. Phys.* **1976**, *64*, 2695−2696.
(45) Tanabe, K.; Saëki, S. Vibrational frequencies, infrared absorption intensities and energy differences between rotational isomers of propyl halides. *J. Mol. Struct.* **1975**, *27*, 79−96.
(46) Tanabe, K. Calculation of infrared band intensities and determination of energy differences of rotational isomers of 1,2-dichloro-, 1,2-dibromo- and 1-chloro-2-bromoethane. *Spectrochim. Acta, Part A* **1972**, *28*, 407−424.

https://dx.doi.org/10.1021/acs.jpcb.0c08630
J. Phys. Chem. B 2020, 124, 11015−11021